

Mechanical and Environmental Properties of {UHP}-{FRCC} Panels Bonded to Existing Concrete Beams

Original

Mechanical and Environmental Properties of {UHP}-{FRCC} Panels Bonded to Existing Concrete Beams / Nishiwaki, Tomoya; Mancinelli, Oscar; Fantilli, ALESSANDRO PASQUALE; Adachi, Yuka. - In: SUSTAINABILITY. - ISSN 2071-1050. - ELETTRONICO. - 13:6(2021), p. 3085. [10.3390/su13063085]

Availability:

This version is available at: 11583/2874490 since: 2021-03-15T16:34:12Z

Publisher:

MDPI

Published

DOI:10.3390/su13063085

Terms of use:

openAccess




This article is made available under terms and conditions as specified in the corresponding bibliographic description in the repository

Publisher copyright

(Article begins on next page)

Article

Mechanical and Environmental Properties of UHP-FRCC Panels Bonded to Existing Concrete Beams

Tomoya Nishiwaki ¹, Oscar Mancinelli ², Alessandro Pasquale Fantilli ^{2,*} and Yuka Adachi ¹

¹ Department of Architecture and Building Science, School of Engineering, Tohoku University, Sendai 980-8579, Japan; tomoya.nishiwaki.e8@tohoku.ac.jp (T.N.); yuka.adachi.t8@dc.tohoku.ac.jp (Y.A.)

² Department of Structural, Building and Geotechnical Engineering (DISEG), Politecnico di Torino, 10129 Torino, Italy; oscar.mancinelli@polito.it

* Correspondence: alessandro.fantilli@polito.it; Tel.: +39-011-0904900

Abstract: Among the techniques used to retrofit existing reinforced concrete structures, methods involving Ultra High Performance Fiber Reinforced Cementitious Composites (UHP-FRCC) are widely regarded. However, current practices make the use of this material for in-situ application expensive and complicated to perform. Accordingly, a new method to strengthen existing concrete beams by applying a precast UHP-FRCC layer on the bottom side are introduced and described herein. Two test campaigns are performed with the aim of defining the best conditions at the interface between the reinforcing layer and the existing beam and to reducing the environmental impact of UHP-FRCC mixtures. As a result, the eco-mechanical analysis reveals that the best performances are attained when the adhesion at interface is enhanced by means of steel nails on the upper surface of the UHP-FRCC layer, in which 20% of the cement is replaced by fly ash.

Keywords: existing beams; retrofitting method; environmental assessment; fly ash; moment–curvature relationship; precast elements



Citation: Nishiwaki, T.; Mancinelli, O.; Fantilli, A.P.; Adachi, Y. Mechanical and Environmental Properties of UHP-FRCC Panels Bonded to Existing Concrete Beams. *Sustainability* **2021**, *13*, 3085. <https://doi.org/10.3390/su13063085>

Academic Editor: Fausto Minelli

Received: 5 February 2021

Accepted: 5 March 2021

Published: 11 March 2021

Publisher's Note: MDPI stays neutral with regard to jurisdictional claims in published maps and institutional affiliations.



Copyright: © 2021 by the authors. Licensee MDPI, Basel, Switzerland. This article is an open access article distributed under the terms and conditions of the Creative Commons Attribution (CC BY) license (<https://creativecommons.org/licenses/by/4.0/>).

1. Introduction

Several studies aim at finding the best way to strengthen concrete columns and beams. Among the possible solutions, reinforced concrete (RC) jackets and steel cages are the most used [1,2]. Additionally, jacketing using innovative materials, such as Fiber Reinforced Polymer (FRP) [3–5] and Ultra High-Performance Fiber-Reinforced Cementitious Composites (UHP-FRCC) [6–8], have been successfully introduced and applied in the last decades. In particular, UHP-FRCCs have also brought the interest of many researchers, who assert that for both new and existing structure a new construction era has started [9]. In addition to the high tensile and compressive strength, UHP-FRCC has remarkable water-proofing properties, and therefore can protect structures not only from water, but also from aggressive agents.

Cast-in-situ coating layers, made of UHP-FRCC and cured at ambient conditions, are used to enhance the bearing capacity and stiffness of existing RC beams [10], and to repair those damaged as well [11]. Nevertheless, this strengthening procedure requires laborious formworks and long casting procedures compared to the use of FRP. In addition, it is not easy to apply cast-in-situ layers on the bottom of beams because of the gravity action. For these reasons, some studies have been devoted to the mechanical performance of precast HP-FRCC slabs [12] used for strengthening RC structures. For instance, Jongvivatsakul et al. significantly increased the shear capacity of RC beams when Steel Fiber-Reinforced Precast Panels are applied on the faces [13].

However, when a cast-in-situ or precast panel overlays an existing structure, the effectiveness of the strengthening depends on the bond condition at the interface between new and old structures. To avoid the delamination phenomena produced by a weak adhesion, roughening treatments of the existing concrete surfaces ensure better performances than

using bonding agents, such as epoxy resin [14]. In particular, sandblasting and chipping enable a higher surface roughening than grooves and drill holes [15]. Moreover, the environmental impact of the reinforcing layers made with UHP-FRCC is also an important aspect that has been taken into consideration. In fact, recent reports indicate that the clinker burning accounts for approximately 4% of the global CO₂ emissions [16]; hence, the cement manufacturing process emits huge amounts of greenhouse gases [17]. As a consequence, the massive content of cement and the presence of large volume of steel fibers make UHP-FRCC a high carbon footprint material. Thus, the Material Substitution Strategy (MSS), which consists of replacing a large part of clinker with mineral additives, can be an effective way to reduce the embodied CO₂ [18].

Accordingly, a new approach for retrofitting concrete structures is proposed herein. It consists of enhancing the resisting bending moment, and therefore the lifespan, of existing concrete beams by adding UHP-FRCC in the tensile zone. The best stratigraphy of the applied materials, made both with cast-in-situ and precast layers, is selected by means of the eco-mechanical analyses. It is a comparative study in which not only the mechanical performances (bearing capacity, bond conditions, etc.), but also the environmental impact of different UHP-FRCC layers are taken into consideration.

2. Materials and Test Procedure

As shown in Figure 1, the new retrofitting method consists of a precast flat layer applied on the tensile zone of an existing RC beam. The layer is hung to the existing structure by means of plugs and screws, leaving an empty gap between the new and the old parts.

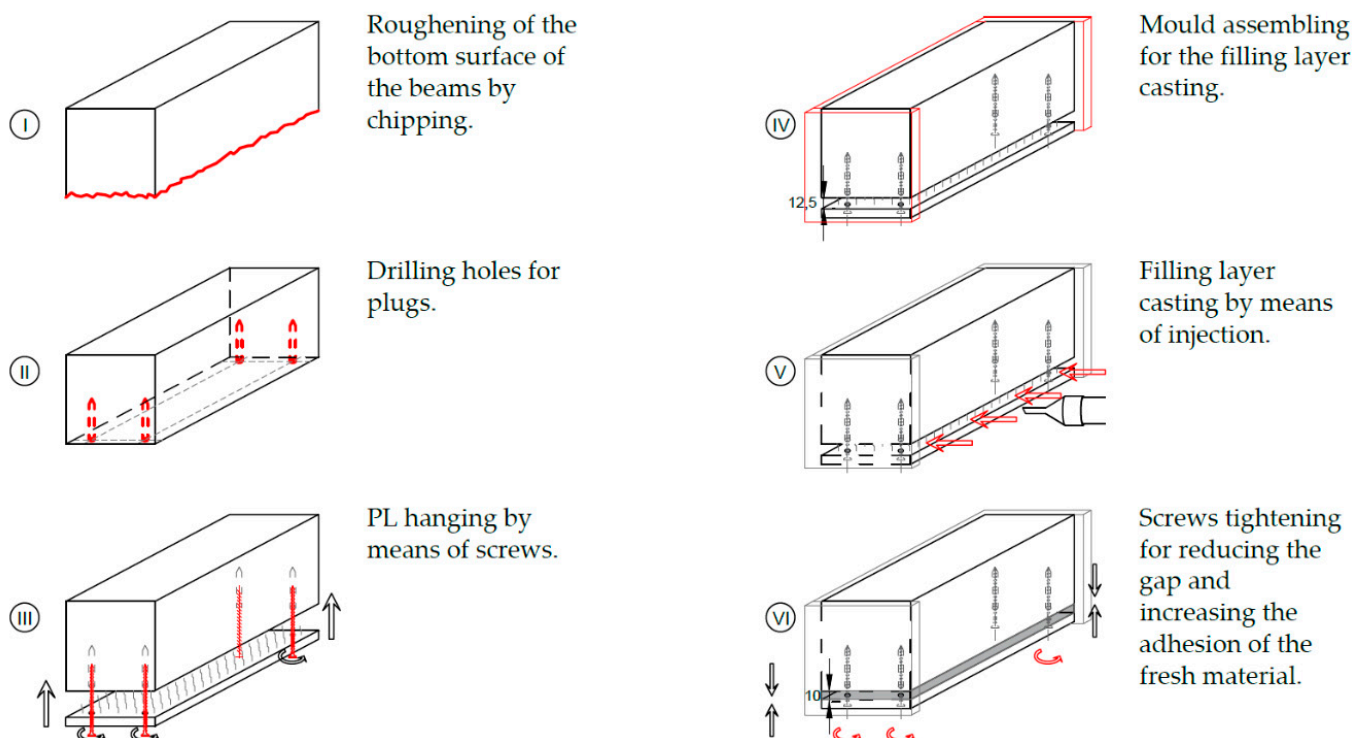


Figure 1. Procedure of strengthening existing beams by applying UHP-FRCC layers.

This gap is then filled by injecting a cement-based mortar. After the injection, a further tightening of the screws tends to reduce the thickness of the gap, and to improve the adhesion between old concrete and the new precast panel.

To have the highest performances of the panel, UHP-FRCC is used. As known, in such a cement-based composite, compressive strength is generally higher than 150 MPa and, in the pre-softening stage, the energy absorption capacity is larger than 50 kJ/m³ [19]. These

performances are achieved not only by adding fibers, but also with a dense microstructure, which is in turn tailored with an extremely low water–binder ratio (lower than 0.2) and by using ultra-fine additive, such as silica fume, wollastonite, and fine sand. Table 1 reports the density of all the materials used to tailor three series of mortar.

Table 1. Materials used to cast the samples (catalog data of producers).

Material	Symbol	Density [kg/m ³]
High Early Strength Portland Cement	HESPC	3140
Low Heat Cement	LHC	3240
Crushed Sand	S1	2610
Land Sand	S2	2580
Silica Fume	SF	2200
Silica Sand	Ss	2600
Wollastonite	Wo	2900
Water	W	1000
Superplasticizer	SP	1050
Defoaming Agent	DA	1010
Macro-fibers (30 mm long)	HDR	7850
Micro-fibers (6 mm long)	OL	7850

Existing beams have been cast with a normal strength mortar, according to mix proportion shown in Table 2. Three UHP-FRCC (namely, FA0, FA20, and FA70) have been used to strengthen the existing beams by means of precast panels. As reported in Table 3, with respect to the reference FA0, containing only cement and silica fume as a binder, in the mix proportions of FA20 and FA70, 20% and 70% of cement have been replaced by fly ash, respectively. Finally, the mix design of the filler layer is shown in Table 4. To reduce the viscosity and facilitate the injection, this filler is obtained from FA0 by removing only macro-fibers.

Table 2. Composition of the normal strength mortar simulating the existing beams (kg per m³ of concrete).

HESPC	S ¹	W
485.6	1456.7	291.4

¹ S = S1 (50% weight) + S2 (50% weight).

Table 3. Composition of the retrofitting UHP-FRCC layers.

Series	W ¹	LHC ¹	SF ¹	FA ¹	Ss ¹	Wo ¹	SP ¹	DA ¹	HDR ²	OL ²
FA0	201	1197	263	0	511	190	32.1	0.3	1.5	1
FA20	195	928	255	232	495	184	31.0	0.3	1.5	1
FA70	181	323	236	753	459	170	31.5	0.3	1.5	1

¹ kg per m³ of concrete., ² % Vol of concrete.

Table 4. Composition of the filler layer.

W ¹	LHC ¹	SF ¹	FA ¹	Ss ¹	Wo ¹	SP ¹	DA ¹	HDR ₂	OL ²
201	1197	263	0	511	190	32.1	0.3	0	1

¹ kg per m³ of concrete., ² % Vol of concrete.

The mechanical properties of all the mixtures are reported in Table 5. Compressive strength and Young's modulus have been determined by testing cylindrical samples in uniaxial compression, whereas uniaxial tensile tests on dumbbell shaped specimens have been performed to measure tensile strength [20].

Table 5. Mechanical proprieties of the concrete (MPa).

Parameter	Normal Strength Mortar	FA0	FA20	FA70
Compressive strength	45.1	204.7	193.4	150.7
Young's modulus	24.9×10^3	46.4×10^3	45.5×10^3	40.1×10^3
Tensile strength	2.6	16.5	17.8	7.4

The use of UHP-FRCC panels is particularly effective in the refurbishment of existing buildings, due to their dual function: structural strengthening and protection against aggressive agents. Nevertheless, due to the high cost and to the environmental impact, UHP-FRCC panels are not used to cover the entire perimeter of the cross-section, or through a three-side jacket [21], but rather they are located only the bottom part of a RC beam. Accordingly, in this research project, small-size beams with a UHP-FRCC layer in the tensile zone (Figure 2a) are investigated with two different tests of Campaign 1 and Campaign 2. Campaign 1 aimed at measuring the effects of four precast reinforcing UHP-FRCC layers (i.e., Type 1—flat slab; Type 2—flat slab with steel nails; Type 3 and Type 4—ribbed slabs), as shown in Figure 2b.

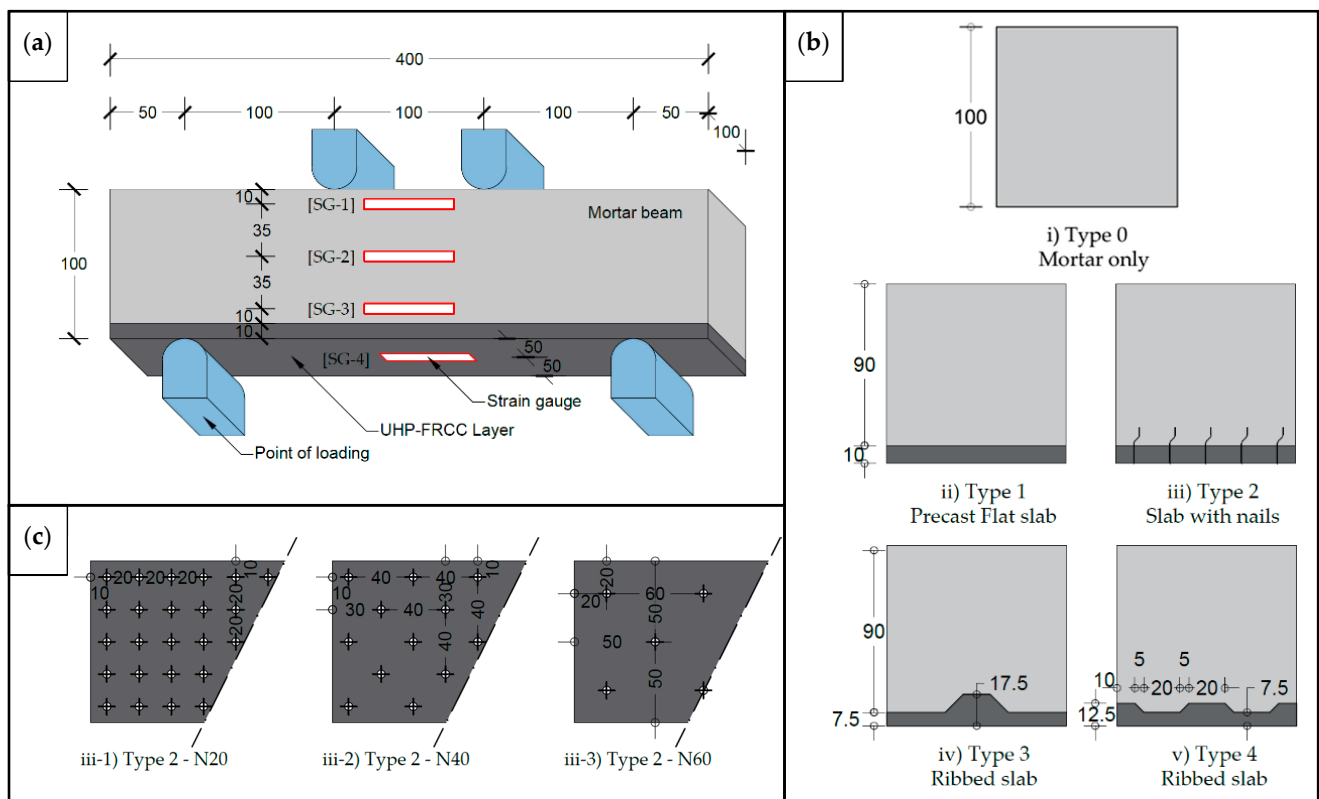


Figure 2. Mortar beams retrofitted by precast UHP-FRCC layer in Test Campaign 1. (a) Specimens shape, strain gauges arrangement, and test configuration. (b) Types of precast layer; (c) Neil density on the surface of the Type 2 precast layer for improving the connection with the mortar beam.

In the case of Type 2 layer, three different bond conditions (namely, N20, N40, and N60 in Figure 2c) are created with the aim of changing the bond conditions between the precast layer and the existing beam. Indeed, in the first phase of this research project, the performance provided by precast layers of different shape and bond condition has to be investigated. Thus, the assembling technique illustrated in Figure 1 is not used. On the contrary, normal strength mortar (see Table 2), reproducing the existing beam, has been

directly cast on precast UHP-FRCC layer made with FA0 (see Table 3). For these specimens, the injection between the existing beams and the additional UHP-FRCC is not necessary.

In Campaign 2, the existing beams are reinforced with screws and plugs, following the procedure illustrated in Figure 1. Only Type 2 layer of Figure 2b, which performed better than the other panels, is used. Such layers are cast with three different series of UHP-FRCC (FA0, FA20, and FA70) to reduce the embodied CO₂. The results obtained from these specimens are benchmarked with those of unreinforced beams (Type 0 in Figure 3b) and with the samples representative of the current strengthening method (i.e., Type 5 in Figure 3b). It consists of a UHP-FRCC layer cast-in-situ on the surface of the beam, without any screws and plugs.

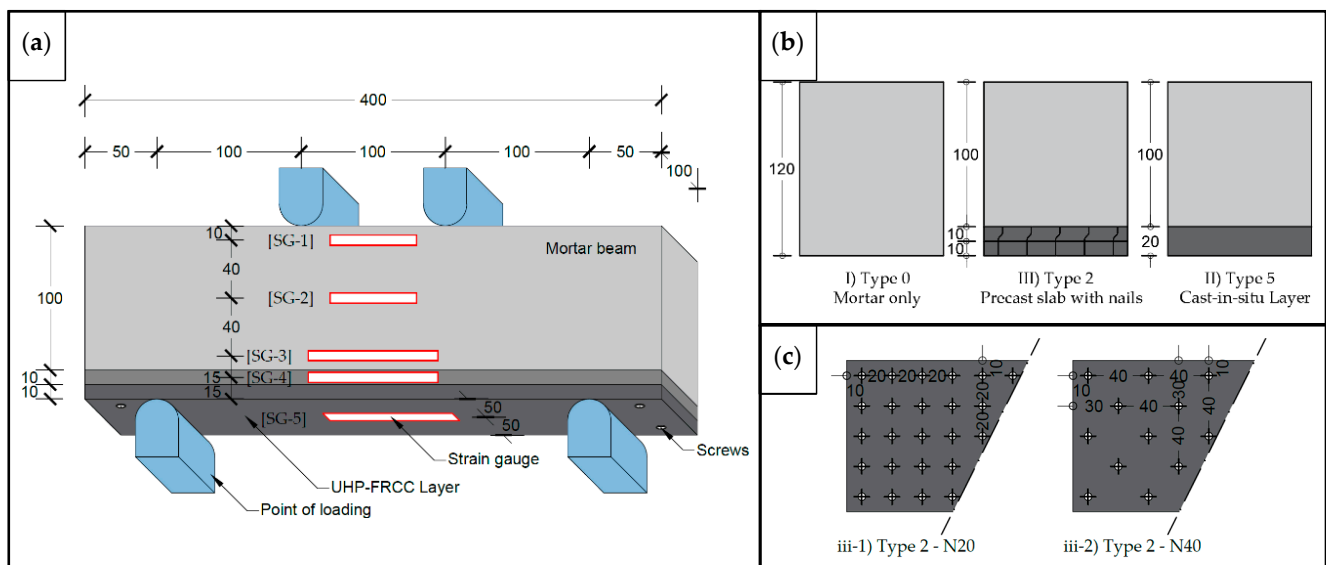


Figure 3. Mortar beams retrofitting by UHP-FRCC layer. (a) Specimens shape, strain gauges arrangement, and test configuration regarding the second test campaign; (b) Precast UHP-FRCC layers used to reinforce the beams; (c) Nail density on the surface of the type 2 precast layers for improving the connection between the parts.

3. Test Campaign 1

3.1. Specimens and Test Setup

Figure 2a illustrates the specimens tested in Campaign 1, which consist of mortar (Table 2) beams retrofitted with a precast UHP-FRCC layer. The thickness of the layer is 10 mm, whereas 100 mm is the depth of the beam, and both the layer and the beam are 100 mm wide. The length of the beam is 400 mm. The nails of the Type 2 series consist of hook-end steel fibers, arranged as in Figure 2c (i.e., at a distance of 20 mm—N20 series, of 40 mm—N40 series, and of 60 mm—N60 series) and embedded within the precast layer. Therefore, the parameters measured in this test campaign are the shape of the precast UHP-FRCC layers (Types 1, 2, 3, and 4) and the density of nails in the Type 2 series (N20, N40, and N60). The samples tested in the Campaign 1 are summarized in Table 6, where all the layers have been made with FA0 (see Table 3).

Table 6. Details of the specimens investigated in the Test Campaign 1.

Symbol	Layer Type	Bonding Surface	Number of Samples
B_I_T0	Type 0	[–]	2
B_I_T1	Type 1	Flat	2
B_I_T2_N20	Type 2	Steel fibers—Spacing: 20 mm	2
B_I_T2_N40	Type 2	Steel fibers—Spacing: 40 mm	2
B_I_T2_N60	Type 2	Steel fibers—Spacing: 60 mm	2
B_I_T3	Type 3	Ribbed	2
B_I_T4	Type 4	Ribbed	2

After casting the UHP_FRCC layers, they are steam cured for 48 h at 90 °C (95% RH) [22], and then used to cast the mortar beams. Finally, the composite beams are stored for 28 days in the curing room (at 20 °C and 95% RH).

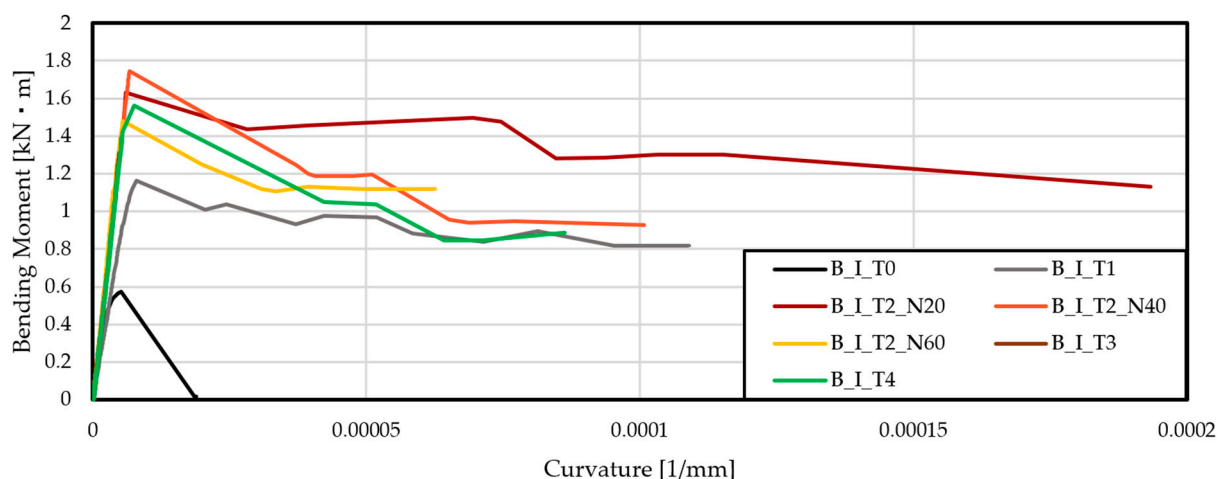
The mechanical performances of the specimens are measured through four-point bending tests performed by using a 1000 kN Universal Testing Machine. A constant speed of 0.3 mm/min of the ram stroke is employed. As shown in Figure 2a, four strain gauges (with a length of 60 mm) are glued on the constant moment zone of the beam. Three of them measured the strains on a single face of the existing beam, whereas the fourth is located on the bottom side (i.e., on the UHP-FRCC layer). Through these strain gauges, the average curvature χ in the constant moment zone is calculated by means of the following equation:

$$\chi = (\varepsilon_4 - \varepsilon_1)/d_0 \quad (1)$$

where ε_4 and ε_1 are the strains measured by the strain gauge [SG-4] (on the bottom side) and [SG-1], respectively, and $d_0 = 90$ mm is the distance between the two gauges.

3.2. Results and Discussion

In Figure 4, the moment–curvature curves of the mortar beam without strengthening (B_I_T0) is put into comparison with those of the beams retrofitted with the different types of precast layers (see Figure 2 and Table 6).

**Figure 4.** Moment–curvature curves measured in the beams of the Test Campaign 1.

Obviously, all beams reinforced with the UHP-FRCC precast layer show a maximum bending moment greater than that of the unreinforced mortar beam. Among them, the beam retrofitted with the precast layer without nails (i.e., B_I_T1) is less strong, whereas the B_I_T2_N20 and B_I_T2_N40 show the highest load-bearing capacity. In fact, the failure of the beams B_I_T2_N20, B_I_T2_N40, and B_I_T3 is due to the failure of the precast layer, whereas B_I_T1 and B_I_T2_N60 beams collapsed after the detachment of the reinforcing layer, which delaminates before exploiting the reinforcing capability. The

density of the nails on the interface between the precast UHP-FRCC layer and mortar beam affects both the load-bearing capacity and the post peak behavior. Indeed, beams strengthened with N40 and N60 Type 2 layers (see Figure 2c) show a more brittle behavior than those reinforced by N20 precast UHP-FRCC.

Figure 5 depicts the strain profiles of the cross-sections, when in the constant moment zone of the beams B_I_T0 (Figure 5a), B_I_T3 (Figure 5b), and B_I_T2_N20 (Figure 5c), two different loads are acting. In all the specimens, plane cross-sections remain plane when 1/3 of the maximum load is applied. Conversely, nonlinear strain profiles can be observed at the ultimate bending moment. Nevertheless, in the bottom of the beam B_I_T2_N20, the strains measured during the tests are larger than those of the linear theoretical trend. The exact opposite occurs in the beams B_I_T0, without reinforcement, and B_I_T3, where the lower real strains indicate a weak transmission of the shear stresses due to the delamination of the UHP-FRCC layer from the mortar beam.

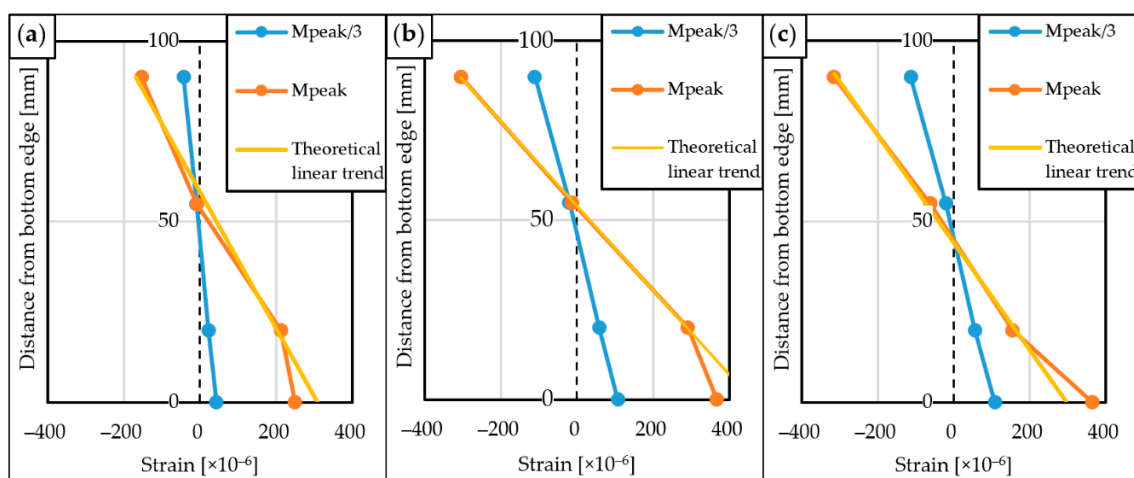


Figure 5. Strain profiles measured in the beams (a) B_I_T0, (b) B_I_T3, and (c) B_I_T2_N20.

This experimental result emphasizes the fundamental role that nails play in the transmission of stresses between the existing beam and the reinforcing layer. As illustrated in Figure 6 where the strain profiles of the beams B_I_T2_N20 (Figure 6a), B_I_T2_N40 (Figure 6b), and B_I_T2_N60 (Figure 6c) are reported, delamination does not occur when nails are present. Accordingly, in the Test Campaign 2, only Type 2 N20 and Type 2 N40 layers were used to reinforce the existing beams.

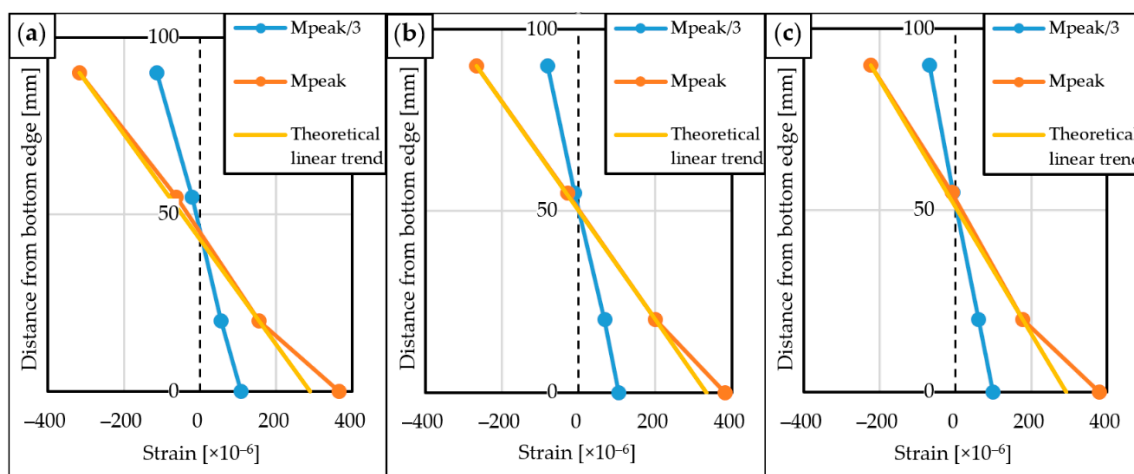


Figure 6. Strain profiles measured in the beams (a) B_I_T2_N20, (b) B_I_T2_N40, and (c) B_I_T2_N60.

4. Test Campaign 2

4.1. Specimens and Test Setup

In this second campaign, mortar beams and precast layers are cast, and the general scheme of Figure 1 is adopted to create the composite structure. Not only the different types of the layers shown in Figure 3b are tested, but also the environmental performances of the UHP-FRCC are analyzed. Such layers have been made by FA0, FA20, and FA70 mixtures shown in Table 3.

The mortar beams have been stored in the curing room for 28 days, whereas the precast layers have been steam cured and then stored in the curing room for the same lapse of time. To simulate the current reinforcing approach, the bottom surfaces of some mortar beams are chipped and subsequently reinforced with a layer of UHP-FRCC cast on the bottom surface, as shown in Figure 3b (Type 5 layer). The remaining mortar beams are strengthened by applying the precast UHP-FRCC layers (Type 2 in Figure 3b,c) by means of chipping, plugs, screws, and the filling layer, as illustrated in Figure 1. Figure 3a shows the general scheme of the 120 mm high specimens tested by means of a 1000 kN Universal Testing Machine, whereas Table 7 summarizes the composite beams investigated in Test Campaign 2. As every type of specimen counted four samples, a total of 40 beams were realized and tested.

Table 7. Details of the specimens tested in the Campaign 2.

Symbol	Layer Type	Bonding Surface	UHP-FRCC Series	Number of Samples
B_II_T0	None	[-]	[-]	4
B_II_T2_FA0_N20	Type 2	Steel fibers—Spacing: 20 mm	FA0	4
B_II_T2_FA0_N40	Type 2	Steel fibers—Spacing: 40 mm	FA0	4
B_II_T2_FA20_N20	Type 2	Steel fibers—Spacing: 20 mm	FA20	4
B_II_T2_FA20_N40	Type 2	Steel fibers—Spacing: 40 mm	FA20	4
B_II_T2_FA70_N20	Type 2	Steel fibers—Spacing: 20 mm	FA70	4
B_II_T2_FA70_N40	Type 2	Steel fibers—Spacing: 40 mm	FA70	4
B_II_T5_FA0	Type 5	Chipping only	FA0	4
B_II_T5_FA20	Type 5	Chipping only	FA20	4
B_II_T5_FA70	Type 5	Chipping only	FA70	4

In all the tests, five strain gauges were glued in the composite beams, one in the lower surface and four on a side face. As shown in Figure 3a, the strain gauges [SG-3], [SG-4] and [SG-5], closer to the bottom, are 90 mm long, and the rest are 60 mm long. By means of these instruments, the strain profile is measured in the cross-section of the constant moment zone, and the debonding phenomena among the layers are also detected. In addition, the measure of the curvature is carried out with the following equation:

$$\chi = (\varepsilon_5 - \varepsilon_1) / d_0 \quad (2)$$

where ε_5 and ε_1 are the strains measured by the strain gauge [SG-5] (on the bottom side) and strain gauge [SG-1], respectively; and $d_0 = 110$ mm is the distance between the two gauges.

4.2. Results and Discussion

Figure 7 shows the average moment–curvature relationships of the reinforced beams, whose strength capacity (i.e., the maximum bending moment) is summarized in the histogram of Figure 8.

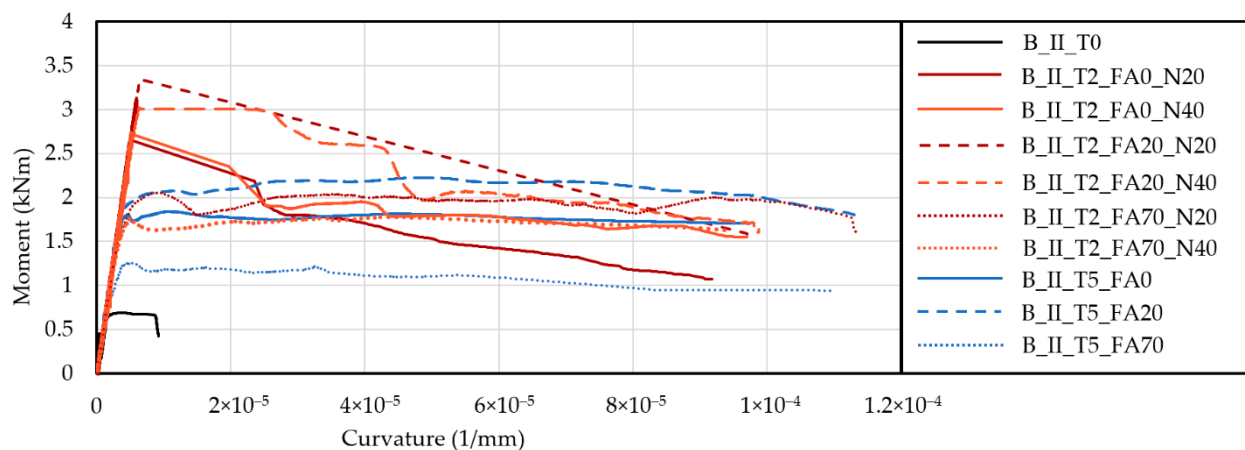


Figure 7. Bending moment–curvature relationship measured in test campaign 2.

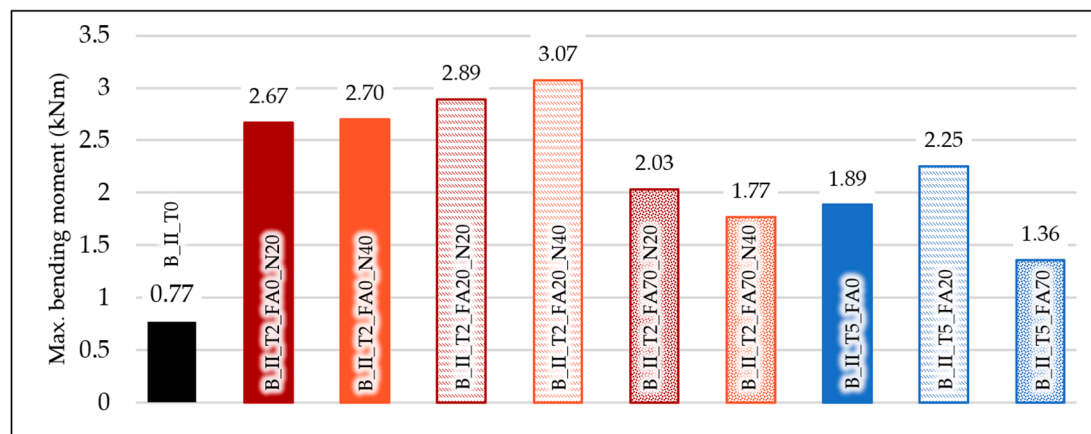


Figure 8. Average values of the maximum bending moment measured in test campaign 2.

Compared to the un-reinforced mortar beam (B_II_T0), a substantial increment of strength and toughness are observed when UHP-FRCC layers are used. However, the maximum bending moment of the beams B_II_T2 is higher than that of B_II_T5, regardless of the class of UHP-FRCC.

Three collapse modes have been identified by linking the stress–strain relationship of UHP-FRCC (obtained from the tensile tests performed on dumbbell shaped specimens) with the moment curvature–relationship (Figure 9):

- Failure in the tensile zone is illustrated in the beams B_II_T2_FA70 and B_II_T5 (Figure 9a). The value of the strain $\varepsilon_{D,y}$ corresponding to the first cracking of the UHP-FRCC substantially coincides with that measured on the bottom of the beam by [SG-5] (see Figure 3a) when first crack occurs. Afterwards, strain hardening appears both in the stress–strain relationship of the reinforcing layer and in the moment curvature relationship. At the peak of bending moment $M_{B,u}$, the strain gauge [SG-5] measured a value ε_5 equal to $\varepsilon_{D,u}$, which is the strain at the tensile strength $\sigma_{D,u}$ of UHP-FRCC. In other words, the ductile behavior of these beams strictly depends on the mechanical performances of the precast layer.
- Figure 9b illustrates the failure due to the crushing of mortar in the compressed zone of the beam. Indeed, during the strain hardening behavior of the UHP-FRCC layer, the moment–curvature relationship shows a softening branch. The resisting area in compression reduces due to the crushing, whereas in the precast layer, wide cracks are visible. In this case, the bending moment corresponding to the first crack, $M_{B,y}$, coincides with that at the peak $M_{B,u}$. This brittle behavior, which generally occurs

in over-reinforced concrete beams, can be observed in the beams B_II_T2_FA0 and B_II_T2_FA20_N40.

- Shear failure (Figure 9c) with a sudden drop in resistance. This brittle behavior is evident in the moment curvature diagram of the beams B_II_T2_FA20_N20, where a diagonal crack appears without crossing the strain gauges of the constant moment zone. As strain localizes in this crack, a reduction of the strain is measured by the gauges before reaching the cracking stress (and strain) in the reinforcing UHP-FRCC layer.

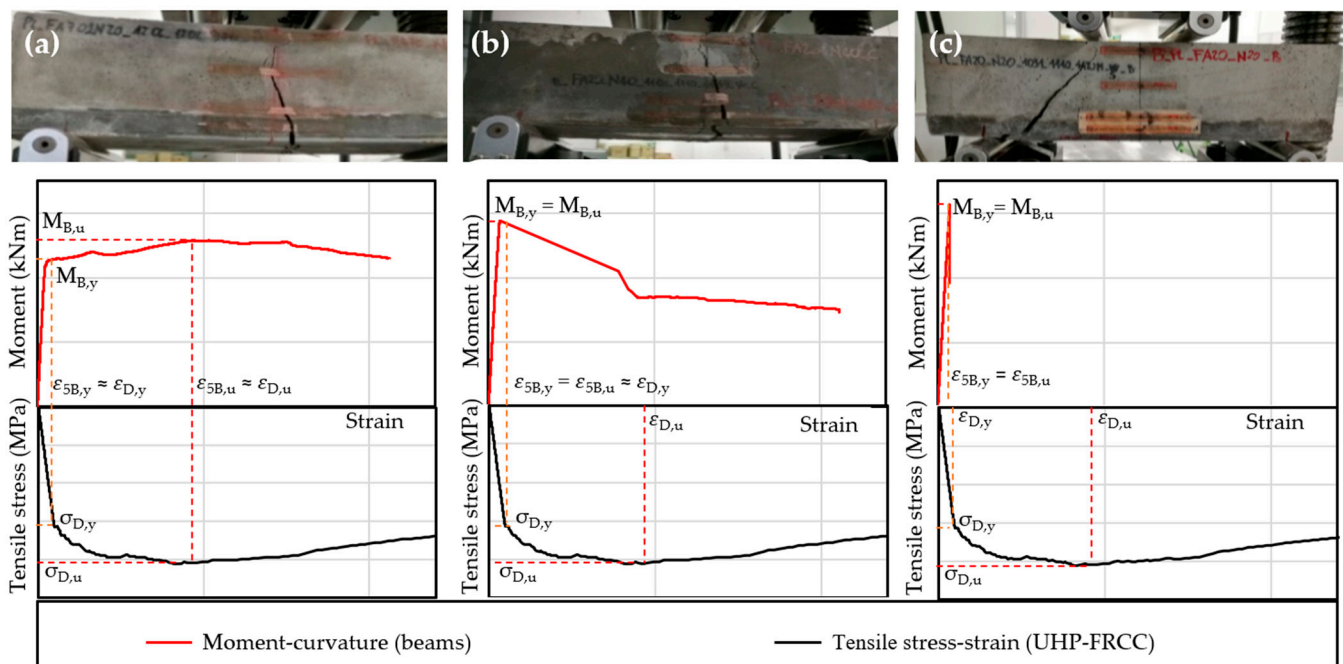


Figure 9. Failures of the beams in the test campaign 2: (a) failure in tension; (b) crushing in the compression zone; (c) shear failure.

Accordingly, the use of high-strength precast layers (such as FA0 and FA20) leads to the brittle behavior of the composite beams, either due to the crushing of mortar in the compression zone, or to the shear failure, especially in the presence of high bond strength (i.e., N20 series). Concerning the content of fly ash, low percentages of this industrial waste (i.e., FA20) produce an increment of strength in the UHP-FRCC layer, but a brittle behavior of the composite beam. On the contrary, the load-bearing capacity of the layer significantly reduces if the substitution rate of cement as fly ash increases (i.e., FA70), but the composite beams show a greater ductility.

To check the effectiveness of the three different types of bond between the reinforcing layer and the existing structure (see Figure 3), the strain profiles of the composite beams B_II_T2_N20, B_II_T2_N40, and B_II_T5 are illustrated in Figure 10. Except for the beam B_II_T5, plane sections remain plane up to the maximum bending moment. As a matter of fact, Figure 10c shows delamination between the mortar and the strengthening layer, which is prevented by combining screws and nails on the surface of the precast UHP-FRCC layer (i.e., Type 2—N20 and Type 2—N40 in Figure 3b,c).

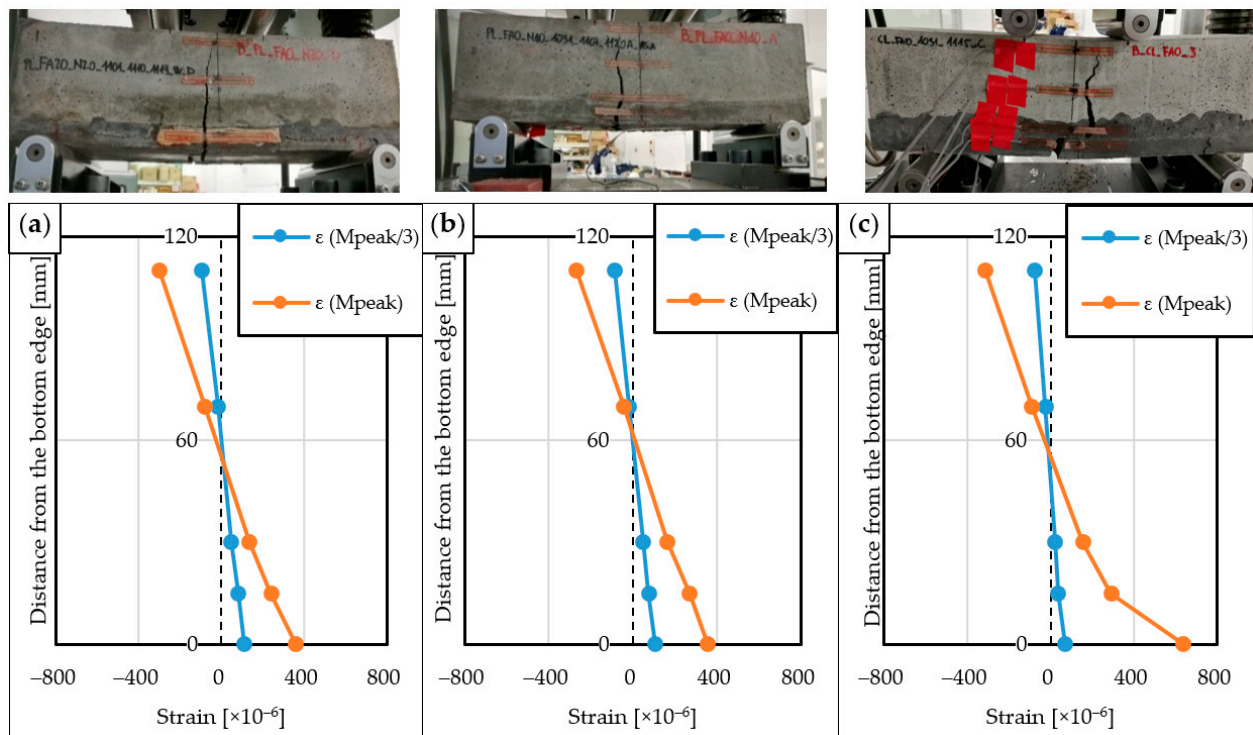


Figure 10. Strain profiles measured in the beams: (a) B_II_T2_N20, (b) B_II_T2_N40, and (c) B_II_T5.

5. Eco-Mechanical Analysis

A further study regarding Test Campaign 2 is herein performed by measuring the environmental performances of the beams, through the so-called eco-mechanical analysis [23]. Using the non-dimensional diagram of Figure 11, a comparative analysis among the beams is carried out in order to select the best reinforcing system, which contemporarily satisfies the environmental and mechanical performances.

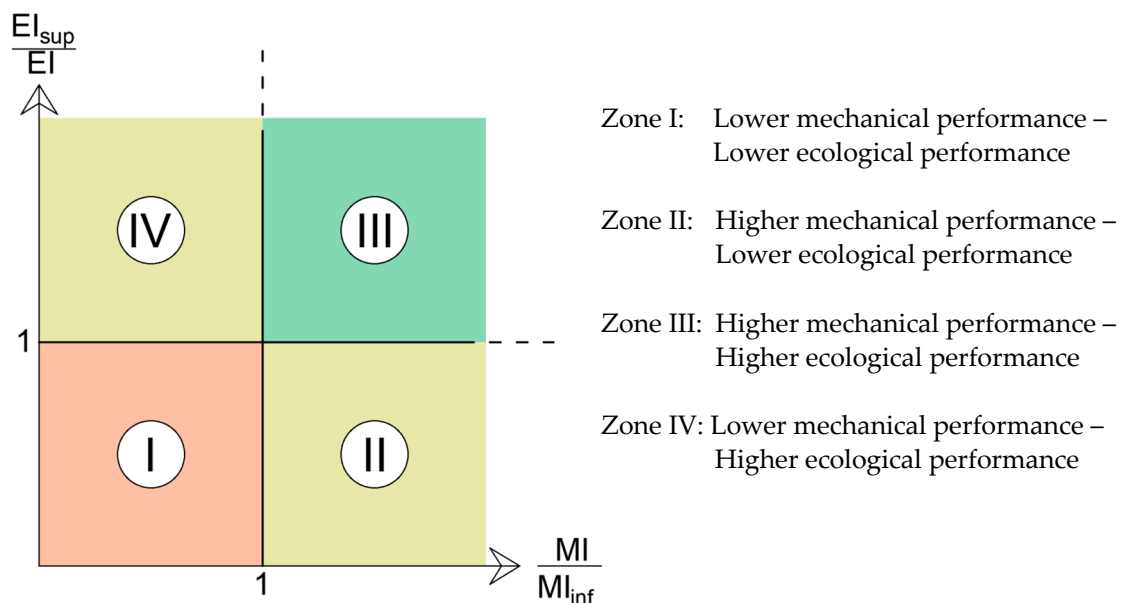


Figure 11. The non-dimensional diagram for evaluating the eco-mechanical performance of specimens.

The horizontal axis of Figure 11 reports the ratio between mechanical indexes (MI/MI_{inf}), whereas the vertical axis represents the ratio between ecological indexes (EI_{sup}/EI). Specif-

ically, MI_{inf} is the lower bound value of mechanical performance, which is the so-called functional unit. In this study, MI_{inf} corresponds to the mechanical performance of a reference series. Similarly, EI_{sup} is the upper bound value of the environmental performance, corresponding to that of the layers of the reference series. In particular, the environmental impact was computed by multiplying the amount of materials used for each type of layer by the relevant unit carbon footprint, as given by the inventory data issued by the Japanese Concrete Institute (JCI) [24]. This computation is consistent with fib [25], where only the CO_2 released in the atmosphere has been taken into account.

The mechanical index, or the functional unit, could be the maximum bending moment in the moment–curvature relationship [26]. On the other hand, according to Fib [25], the mechanical index should also consider the overall behavior of the structure, including the ductility. Therefore, two different parameters are considered herein. The first parameter is the peak of bending moment, whereas in the second parameter (i.e., the ductility) is correlated to the work of deformation per unit length (J/m). It is the area D, defined by the moment–curvature diagram up to the maximum bending moment, as illustrated in Figure 12. Accordingly, it vanishes in the case of brittle behavior (see Figure 9b,c).

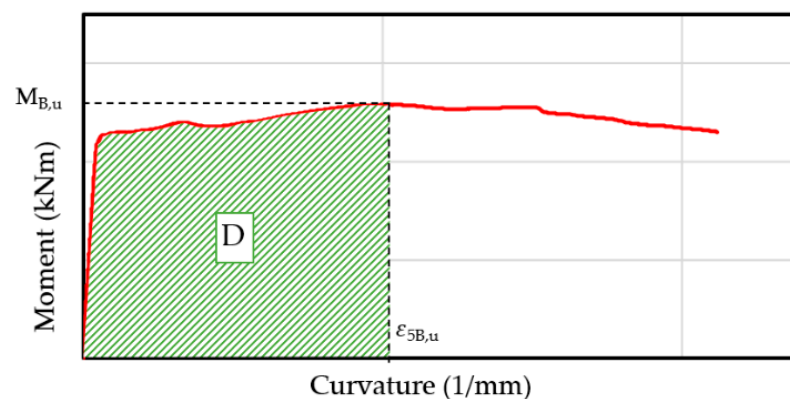


Figure 12. Evaluation of the mechanical indexes.

To calculate MI_{inf} and EI_{sup} , the mechanical and ecological performances of the beam B_II_T5_FA0 are considered as the references, because it represents the current method of retrofitting the existing RC beams. In this beam, UHP-FRCC does not include any supplementary cementitious materials to reduce the carbon footprint. Table 8 summarizes the values of the parameters of each retrofitting layer used to reinforce the beams. The embodied CO_2 computed for the B_II_T2 series also takes into account nails, screws, and the filling layers made with UHP-FRCC without fly ash (FA0). As a result, the environmental indicators are fairly high, even for the Type 2—FA20 and FA70 series. An additional reduction in CO_2 emission for the FA20 and FA70 series could be achieved by replacing the fly ash in the filling layer.

Table 8. Parameters used for computing the environmental and mechanical indexes.

Parameter	B_II_T2_FA0_		B_II_T2_FA20_		B_II_T2_FA70_		B_II_T5_		
	N20	N40	N20	N40	N20	N40	FA0	FA20	FA70
M_{peak} (kNm)	2.67	2.70	2.89	3.07	2.03	1.77	1.89	2.25	1.36
D. Work(J/m)	0.00	0.00	0.00	0.00	58.87	45.20	125.29	70.23	22.45
CO_2 (kg)	0.9719	0.9634	0.8882	0.8797	0.7045	0.6960	0.9679	0.8006	0.4331

All the values are reported within the non-dimensional diagram of Figure 13. In particular, the maximum bending moment is the functional unit in Figure 13a, whereas in Figure 13b, the functional unit is D.

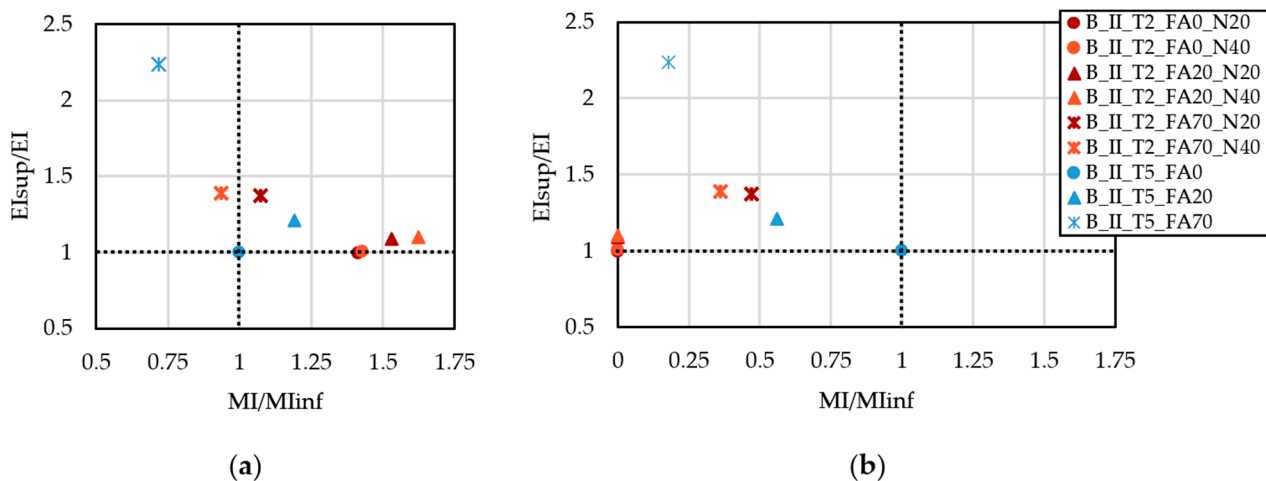


Figure 13. Mechanical and environmental assessment of the precast UHP-FRCC layers by considering (a) MI = maximum bending moment and (b) MI = work of deformation.

Figure 13a points out that the best result in terms of mechanical performances is achieved by the beam B_II_T2_FA20. On the other hand, B_II_T2_FA70 attains a fair reduction in emissions by preserving, approximately, the same resistance of the beam B_II_T5_FA0. When the work of deformation per unit length is the functional unit (see Figure 13b), the beams do not show any increment of ductility with respect to the reference beam B_II_T5_FA0. In particular, the beams B_II_T2_FA0_N40 and B_II_T2_FA20_N40 exhibited brittle failures, as shown in Figure 9b,c. Hence, their mechanical index MI is zero in Figure 13b.

As this brittle behavior generally affects the over reinforced beams under bending actions, it could be ascribed to the large thickness of the reinforcing UHP-FRCC layer. Thus, further numerical and experimental analyses have to be performed in order to also define the optimal geometry of the precast retrofitting layer, ensuring the strengthening in terms of both resisting bending moment and ductility.

6. Conclusions

The experimental results previously described lead to the following conclusions:

- The delamination failure of the strengthened beam can be avoided by introducing steel nails at the interface between the existing beam and the UHP-FRCC reinforcing layer.
- In addition to nails, the existing beams reinforced with screws and plugs show an increment of the resisting bending moment, regardless of the mixture used to cast the UHP-FRCC layer.
- The eco-mechanical analysis of the composite beams reveals that part of the cement used to cast UHP-FRCC layers can be effectively substituted by fly ash. When the rate of substitution is about 20%, both the environmental impact and the strength of the beams improve. Thus, with the strengthening procedure illustrated in Figure 1, a significant reduction of greenhouse emissions can be obtained while maintaining the mechanical performance provided by the current retrofitting method.
- On the other hand, when the resistance of the reinforcing layer is much higher than that of the existing beam, composite cross-section fails in a brittle manner. To avoid this undesired behavior, which generally occurs in over-reinforced concrete beams in bending, a suitable thickness of the UHP-FRCC layer has to be designed.

Author Contributions: Conceptualization: T.N. and A.P.F.; methodology: T.N., O.M., and A.P.F.; investigation: O.M. and Y.A.; resources: T.N.; data curation: O.M. and Y.A.; writing—original draft preparation: Y.A. and O.M.; writing—review and editing: T.N. and A.P.F.; visualization: O.M. and Y.A.; project administration: T.N., and A.P.F.; funding acquisition: T.N. and A.P.F. All authors have read and agreed to the published version of the manuscript.

Funding: This research received no external funding.

Institutional Review Board Statement: Not applicable.

Informed Consent Statement: Not applicable.

Data Availability Statement: The data presented in this study are available on request to the first author or corresponding author.

Acknowledgments: The authors would like to thank the Italian Civil Protection for the administrative and technical support given within the Research Program DPC Reluis—Politecnico di Torino (2019–2021)—WP11: Code rules contributions in the field of existing reinforced concrete structures.

Conflicts of Interest: The authors declare no conflict of interest.

References

1. Júlio, E.S.; Branco, F.; Silva, V.D. Structural rehabilitation of columns with reinforced concrete jacketing. *Prog. Struct. Eng. Mater.* **2003**, *5*, 29–37. [CrossRef]
2. Adam, J.M.; Ivorra, S.; Pallarés, F.J.; Giménez, E.; Calderón, P.A. Axially loaded RC columns strengthened by steel caging. Finite element modelling. *Constr. Build. Mater.* **2009**, *23*, 2265–2276. [CrossRef]
3. Olivova, K.; Bilcikm, J. Strengthening of concrete columns with CFRP. *Slovak J. Civ. Eng.* **2009**, *17*, 1–9.
4. Dasgupta, A. Retrofitting of concrete structure with fiber reinforced polymer. *Int. J. Innov. Res. Sci. Tech.* **2018**, *4*, 42–49.
5. Irshidat, M.; Al-Saleh, M.H. Strengthening RC columns using carbon fiber reinforced epoxy composites modified with carbon nanotubes. *Int. J. Civ. Struct. Constr. Arch. Eng. Dubai UAE* **2015**, *9*, 19–22.
6. Tayeh, B.A.; Bakar, B.H.A.; Johari, M.A.M.; Voo, Y.L. Utilization of ultra-high performance fibre concrete (Uhpfc) For rehabilitation—A review. *Proc. Eng.* **2013**, *54*, 525–538. [CrossRef]
7. Fantilli, A.P.; Meloni, L.P.; Nishiwaki, T.; Igarashi, G. Tailoring confining jacket for concrete column using ultra high performance-fiber reinforced cementitious composites (UHP-FRCC) With high volume fly ash (HVFA). *Materials* **2019**, *12*, 4010. [CrossRef] [PubMed]
8. Gholampour, A.; Hassanli, R.; Mills, J.E.; Vincent, T.; Kunieda, M. Experimental investigation of the performance of concrete columns strengthened with fiber reinforced concrete jacket. *Constr. Build Mater.* **2019**, *194*, 51–61. [CrossRef]
9. Brühwiler, E. “Structural UHPFRC”: Welcome to the post-concrete era! In Proceedings of the First International Interactive Symposium on UHPC, Iowa State University, Ames, IA, USA, 18–20 July 2016.
10. Ruano, G.; Isla, F.; Pedraza, R.I.; Sfer, D.; Luccioni, B. Shear retrofitting of reinforced concrete beams with steel fiber reinforced concrete. *Constr. Build. Mater.* **2014**, *54*, 646–658. [CrossRef]
11. Martinola, G.; Meda, A.; Plizzari, G.A.; Rinaldi, Z. Strengthening and repair of RC beams with fiber reinforced concrete. *Cem. Concr. Compos.* **2010**, *32*, 731–739. [CrossRef]
12. Junior, P.R.R.S.; Maciel, P.S.; Barreto, R.R.; Neto, J.T.D.S.; Corrêa, E.C.S.; Bezerra, A.C.D.S. Thin slabs made of high-performance steel fibre-reinforced cementitious composite: Mechanical behaviour, statistical analysis and microstructural investigation. *Materials* **2019**, *12*, 3297. [CrossRef] [PubMed]
13. Jongvivatsakul, P.; Bui, L.V.H.; Koyekaewphring, T.; Kunawisarut, A.; Hemstapat, N.; Stitmannaitum, B. Using steel fiber-reinforced concrete precast panels for strengthening in shear of beams: An experimental and analytical investigation. *Adv. Int. Civ. Eng.* **2019**, *2019*, 4098505. [CrossRef]
14. Júlio, E.N.B.S.; Branco, F.A.B.; Silva, V.D. Concrete-to-concrete bond strength: Influence of an epoxy-based bonding agent on a roughened substrate surface. *Mag. Concr. Res.* **2005**, *57*, 463–468. [CrossRef]
15. Malek, N.A.A.A.; Muhamad, K.; Zahid, M.Z.A.M.; Hamiruddin, N.A.; Zainol, N.Z.; Yahya, N.; Bahaman, N.; Ramli, N.M. Evaluation of Bond Strength Between Normal Concrete and High Performance Fiber Reinforced Concrete (HPFRC). In Proceedings of the MATEC Web of Conferences 195, Solo Baru, Indonesia, 11–12 July 2018.
16. Oliver, J.G.J.; Peters, J.A.H.W. *Trends in Global CO₂ and Total Greenhouse Gas Emissions*; PBL Netherlands, Environmental Assessment Agency: The Hague, The Netherlands, 2020.
17. Damineli, B.L.; Kemeid, F.M.; Aguiar, P.S.; John, V.M. Measuring the eco-efficiency of cement use. *Cem. Concr. Compos.* **2010**, *32*, 555–562. [CrossRef]
18. Habert, G.; Roussel, N. Study of two concrete mix-design strategies to reach carbon mitigation objectives. *Cem. Concr. Compos.* **2009**, *31*, 397–402. [CrossRef]
19. Wille, K.; El-Tawil, S.; Naaman, A. Properties of strain hardening ultra high performance fiber reinforced concrete (UHP-FRC) under direct tensile loading. *Cem. Concr. Compos.* **2014**, *48*, 53–66. [CrossRef]
20. Japan Society of Civil Engineers (JSCE). Recommendations for Design and Construction of HPFRCC with Multiple Fine Cracks. 2018. Available online: http://www.jsce.or.jp/committee/concrete/e/hpfrcc_JSCE.pdf (accessed on 9 March 2021).
21. Lampropoulos, A.P.; Paschalis, S.A.; Tsioulou, O.T.; Dritsos, S.E. Strengthening of reinforced concrete beams using ultra high performance fibre reinforced concrete (UHPFRC). *Eng. Struct.* **2015**, *106*, 370–384. [CrossRef]

22. Kwon, S.; Nishiwaki, T.; Kikuta, T.; Mihashi, H. Development of ultra-high-performance hybrid fiber-reinforced cement-based composites. *ACI Mater. J.* **2014**, *111*. [[CrossRef](#)]
23. Fantilli, A.P.; Chiaia, B. The work of fracture in the eco-mechanical performances of structural concrete. *J. Adv. Concr. Technol.* **2013**, *11*, 282–290. [[CrossRef](#)]
24. Japan Concrete Institute. *A Textbook of Environmental Aspects for Concrete, Outline of Lci Data of Cement*; Japan Concrete Institute: Tokyo, Japan, 2013.
25. International Federation for Structural Concrete. *Guidelines for Green Concrete Structures*; FIB Bulletin No. 67; FIB Bulletin: Lausanne, Switzerland, 2012.
26. Flower, D.J.M.; Sanjayan, J.G. Green house gas emissions due to concrete manufacture. *Int. J. Life Cycle Ass.* **2007**, *12*, 282–288. [[CrossRef](#)]